

Surface effects in color superconducting strange-quark matter

Micaela Oertel

LUTH, Observatoire de Paris, CNRS, Université Paris Diderot, 5 place Jules Janssen, 92195 Meudon, France

Michael Urban

IPN Orsay, CNRS-IN2P3 and Université Paris-Sud, 91406 Orsay cedex, France

Surface effects in strange-quark matter play an important role for certain observables which have been proposed in order to identify strange stars, and color superconductivity can strongly modify these effects. We study the surface of color superconducting strange-quark matter by solving the Hartree-Fock-Bogoliubov equations for finite systems (“strangelets”) within the MIT bag model, supplemented with a pairing interaction. Due to the bag-model boundary condition, the strange-quark density is suppressed at the surface. This leads to a positive surface charge, concentrated in a layer of ~ 1 fm below the surface, even in the color-flavor locked (CFL) phase. However, since in the CFL phase all quarks are paired, this positive charge is compensated by a negative charge, which turns out to be situated in a layer of a few tens of fm below the surface, and the total charge of CFL strangelets is zero. We also study the surface and curvature contributions to the total energy. Due to the strong pairing, the energy as a function of the mass number is very well reproduced by a liquid-drop type formula with curvature term.

PACS numbers: 21.65.Qr,12.39.Ba,26.60.-c

I. INTRODUCTION

From rather general arguments it is expected that at low temperatures and high densities quark matter is in a color superconducting state [1]. More recently [2, 3] it has been suggested that the diquark pairing gaps for quark matter at densities of several times nuclear matter saturation density could be of the order of ~ 100 MeV. Since this could have important phenomenological consequences in particular for the interior of compact stars, this has triggered much work on color superconductivity in dense quark matter (for reviews, see, e.g., Ref. [4]). These investigations of the QCD phase diagram have revealed a very rich phase structure with many different possible pairing patterns, depending on external conditions such as, for instance, electrical neutrality or quark masses. The largest diquark pairing gaps arise from scalar condensates, leading either to the two-flavor color superconducting (2SC) phase or to the color-flavor-locked (CFL) phase [5, 6]. The latter pairing pattern involves strange (s) quarks, in addition to the two light quark flavors, up (u) and down (d).

If color superconducting quark matter exists in nature, the most likely place to find it is the interior of compact stars because matter is compressed there to densities much higher than nuclear matter saturation density. However, it has been argued that strange-quark matter (SQM) might be absolutely stable [7]. Under this hypothesis, even pure strange stars should exist [8], i.e., stars entirely composed of SQM. Also small lumps of SQM, called “strangelets,” might be stable. Because of their low charge to baryon number ratio Z/A , strangelets have been proposed to populate ultra-high energy cosmic rays [9].

In SQM without pairing, the density of strange quarks is supposed to be smaller than that of light quarks be-

cause of their higher mass. Consequently, SQM and strangelets are positively charged and the charge neutrality of strange stars has to be achieved via the presence of electrons. At the surface an atmosphere of electrons forms [8] which can potentially be detected [10, 11] via the emission of electron-positron pairs from an extremely strong electric field at the surface.

Recently another possible picture of the surface of a strange star has been proposed [12]: there could be a “crust” composed of strangelets immersed in an electron gas. Similar to an ordinary neutron star, there could be an interface between the crust and the interior in form of the famous “pasta phases.” Within this scenario the electric field at the surface would be strongly reduced. Obviously, surface effects for the strangelets play an important role for the description of this scenario. For instance, there is a critical surface tension deciding whether a homogeneous phase or the droplet phase is favored [13]. Another question for which surface effects should be considered is the formation of a strange star in a supernova explosion. Before the explosion the original star contains hadronic matter. During the formation of the star, nucleation of strangelets sets in, leading then to a conversion of the entire star to SQM. For the nucleation process the properties of small strangelets are important.

Pairing tends to reduce the differences in density of different quark species. For bulk quark matter in the CFL state, requiring color neutrality, all quarks are paired. The densities are thus equal and CFL quark matter is electrically neutral on its own, i.e., without any electrons [14]. This would suggest dramatic changes in the properties of strangelets and SQM inside compact stars. For instance, the electrosphere at the surface of a strange star could completely disappear. But, the presence of the surface can modify this picture since it can lead to a non-zero surface charge which remains even for large

objects. For example, the boundary condition of the MIT bag model suppresses the density of the massive strange quarks at the surface, resulting in a positive surface charge [15]. Within this scenario, the total charge of a strangelet, following roughly $Z \approx 0.3A^{2/3}$, is drastically reduced with respect to “normal” strangelets. For strange stars, this requires the presence of electrons [16]. However, pairing has not been treated self-consistently in previous work (see, e.g., Ref. [15]). In this paper we will therefore reinvestigate finite-size strangelets with pairing by considering quark matter in a color superconducting spherical bag, solving the Hartree-Fock-Bogoliubov (HFB) equations. We will show, in particular, that there exist CFL type solutions where all quarks are paired and the total charge of the strangelet strictly vanishes.

The outline of the paper is as follows. In Section II we will present our model for treating color superconducting quark matter in a finite volume. In Section III we will show numerical results. In Section III A we discuss the possibility of qualitatively different configurations. In Section III B we concentrate on the charge-density distributions of the CFL like solutions. In Section III C we discuss a liquid-drop like mass formula for the CFL-like solutions and calculate the surface tension. Finally, in Section IV we will summarize our results.

II. MODEL

A. Lagrangian

Since it is not possible to describe strangelets or SQM with a surface from first principles (QCD), we will use a quark model which allows to describe finite-size objects. For this purpose we will use here the MIT bag model [17]. The idea of this model is that confinement can be simulated by the existence of a “bag” which consists of a “hole” in the non-perturbative QCD vacuum. Inside this “bag”, the vacuum is supposed to be perturbative, i.e., inside the bag the interactions of the quarks can be treated perturbatively. To create this “hole” in the non-perturbative QCD vacuum, an energy per volume, B , is necessary. In the present work we will consider a static spherical bag with radius R . On the surface of the bag, the quark field ψ has to satisfy an appropriate boundary condition. In the simplest version of the MIT bag model, the boundary condition reads

$$-i\mathbf{e}_r \cdot \boldsymbol{\gamma}\psi = \psi|_{r=R}. \quad (1)$$

which ensures that there is no particle flux across the surface. By $r = |\mathbf{r}|$ we denote the radial coordinate, measured from the center of the bag, and $\mathbf{e}_r = \mathbf{r}/r$ is the radial unit vector. The boundary condition (1) leads to a suppression of the wave functions of massive particles at the surface. This means that the strange-quark density will a priori be suppressed at the surface with respect to the light quark densities.

The MIT bag model can be expressed in terms of a Lagrangian density as follows [18]:

$$\mathcal{L}_{bag} = [\bar{\psi}(i\boldsymbol{\gamma}^\mu\partial_\mu - m)\psi - B]\theta(R - r) - \frac{1}{2}\bar{\psi}\psi\delta(R - r), \quad (2)$$

where m is the matrix of quark masses. Due to the second term, the boundary condition (1) follows immediately from the Euler-Lagrange equation for the quark field [18].

In order to include pairing, we will supplement the bag model with a pairing interaction. In principle, perturbative one-gluon exchange generates an attractive pairing interaction in certain channels, in particular in the scalar color antitriplet channel. For simplicity, we will use here a four-point pairing interaction acting only in this dominant channel. The corresponding Lagrangian reads (see any of the standard review articles on color superconductivity [4])

$$\mathcal{L}_{pair} = H \sum_{A,A'} (\bar{\psi}i\boldsymbol{\gamma}_5\tau_A\lambda_{A'}C\bar{\psi}^T)(\psi^TCi\boldsymbol{\gamma}_5\tau_A\lambda_{A'}\psi), \quad (3)$$

where H is a dimensionful coupling constant, C denotes the charge conjugation matrix, and $\tau_A, \lambda_{A'}$ represent $SU(3)$ matrices in flavor and color space, respectively. We follow the convention that capital letters A, A' indicate that we are restricting τ_A and $\lambda_{A'}$ to be antisymmetric, i.e., in terms of the Gell-Mann matrices, $A, A' \in \{2, 5, 7\}$.

In addition to the strong interaction, the quarks will exhibit electromagnetic interactions which, due to their long range, become particularly important for large objects. The corresponding Lagrangian reads

$$\mathcal{L}_{e.m.} = -\frac{1}{4}F_{\mu\nu}F^{\mu\nu} - e\bar{\psi}QA_\mu\boldsymbol{\gamma}^\mu\psi, \quad (4)$$

where $F_{\mu\nu} = \partial_\mu A_\nu - \partial_\nu A_\mu$ and A_μ denote respectively the electromagnetic field strength tensor and four-potential, and Q is the matrix of quark charges in units of e , $Q_u = 2/3$, $Q_d = Q_s = -1/3$.

It would be in the spirit of the bag model to include also the gluon exchange in a perturbative way, i.e., in the same way as the photon. However, this goes beyond the scope of the present paper and will be postponed to a future study.

B. Solution in the framework of HFB theory

The model described by $\mathcal{L} = \mathcal{L}_{bag} + \mathcal{L}_{pair} + \mathcal{L}_{e.m.}$ will be treated in the framework of HFB theory. By minimizing the energy in mean field approximation (for more details see Appendix B and Ref. [19] where the “Dirac-Hartree-Bogoliubov” approximation was developed for finite nuclei), one obtains the following HFB equations:

$$\begin{pmatrix} h & \Delta \\ \Delta & -h \end{pmatrix} \begin{pmatrix} U_\alpha(\mathbf{r}) \\ \gamma^0 V_\alpha(\mathbf{r}) \end{pmatrix} = \epsilon_\alpha \begin{pmatrix} U_\alpha(\mathbf{r}) \\ \gamma^0 V_\alpha(\mathbf{r}) \end{pmatrix}. \quad (5)$$

The single-particle Hamiltonian

$$h = -i\boldsymbol{\alpha} \cdot \boldsymbol{\nabla} + m\gamma^0 + \Sigma - \mu \quad (6)$$

includes besides the free Dirac Hamiltonian the quark self-energy Σ (in our case due to Coulomb interaction) and the matrix of chemical potentials μ which depend on flavor $f \in \{u, d, s\}$ and color $c \in \{r, g, b\}$ (we will denote the three colors by red, green, and blue). Δ denotes the pairing field (gap). The spinors U_α and V_α describe the particle- and hole-like components of the quark fields, respectively [see Eq. (B3)], where α is a multi-index containing all quantum numbers characterizing a single-particle state (see Appendix A). In writing Eq. (5), we implicitly assumed that the pairing field Δ can be chosen real, which is the case for the pairing pattern we consider, and that the self-energy Σ is local, which is the case since we neglect the exchange (Fock) term (see below).

The pairing field Δ and the self-energy Σ depend themselves on the wave functions U and V , such that we have to solve a self-consistency problem. To be specific, the pairing field Δ depends on the diquark condensates

$$s_{AA'}(x) = -\langle \bar{\psi}_T(x) \tau_A \lambda_{A'} \psi(x) \rangle, \quad (7)$$

where ψ_T denotes the time-reversed conjugate of ψ ,

$$\psi_T = \gamma_5 C \bar{\psi}^T. \quad (8)$$

The diquark condensates can be expressed in terms of the U and V functions as

$$s_{AA'}(r) = - \sum_{\beta, \epsilon_\beta < 0} \bar{V}_\beta(\mathbf{r}) \tau_A \lambda_{A'} U_\beta(\mathbf{r}) \quad (9)$$

(since we are dealing with a static problem, the condensates do not depend on time, and due to spherical symmetry, they depend only on the radial coordinate r). We will limit our investigations here to diagonal condensates, i.e., only condensates with $A = A'$ are non-zero¹. In uniform infinite matter and for an exact $SU(3)$ flavor symmetry, the CFL phase is characterized by nonzero values $s_{22} = s_{55} = s_{77}$, whereas the 2SC state has only $s_{22} \neq 0$. The relation between the condensates s_{AA} and the pairing field Δ reads

$$\Delta(r) = \sum_{A=2,5,7} \Delta_A(r) \tau_A \lambda_A, \quad (10)$$

$$\Delta_A(r) = 2 H s_{AA}(r). \quad (11)$$

In practice, the expression (9) is divergent and it is necessary to introduce a cutoff in order to obtain a finite

result. Since in a finite system the levels are discrete, a sharp cutoff would generate discontinuities as a function of the system's size. We therefore introduce a smooth cutoff function $f(p/\Lambda)$ (see Appendix C for details). Another practical problem arises from antiparticle contributions. However, since the chemical potentials μ_{fc} are large and positive and pairing involves mostly the states near the Fermi surface, we assume that the antiparticle contributions are not important and can be neglected. We checked this approximation (analogous to the “no-sea approximation” in nuclear physics [19]) in infinite matter and found that the effect of antiparticle states can be absorbed in a readjustment of the coupling constant by $\sim 20\%$.

For the normal self-energy Σ we employ the Hartree approximation, i.e., we neglect the Coulomb exchange (Fock) term as well as exchange contributions from the magnetic field. We also disregard the contribution of \mathcal{L}_{pair} to the normal self-energy. Hence, the self-energy is simply proportional to the static Coulomb potential

$$\Sigma(r) = eQ A_0(r) \gamma^0. \quad (12)$$

The Coulomb potential is related to the quark densities by

$$A_0(r) = e \int d^3r' \frac{\rho_{ch}(\mathbf{r}')}{|\mathbf{r} - \mathbf{r}'|}, \quad (13)$$

where

$$\rho_{ch}(r) = \sum_f Q_f \rho_f(r) \quad (14)$$

is the charge density (divided by e), ρ_f being the number density of quarks of flavor f . As it was the case for the diquark condensates, the quark number densities can be expressed in terms of the U and V functions. Denoting by $\tilde{\beta}$ all single-particle quantum numbers except flavor, we can write the number density of quarks of flavor f as

$$\rho_f(r) = \sum_{\tilde{\beta}, \epsilon_{f\tilde{\beta}} < 0} U_{f\tilde{\beta}}^\dagger(\mathbf{r}) U_{f\tilde{\beta}}(\mathbf{r}). \quad (15)$$

Let us now summarize the procedure how the HFB equations are solved. We start with an initial guess for the pairing fields $\Delta_A(r)$ and for the Coulomb potential $A_0(r)$. Then we solve the eigenvalue problem (5) in order to find the U and V functions. From these functions the diquark condensates $s_{AA}(r)$ and the quark densities $\rho_f(r)$ are computed according to Eqs. (9) and (15), which are then used to update the pairing fields Δ_A and the Coulomb field A_0 according to Eqs. (11) and (13). These steps are iterated until convergence (i.e., self-consistency) is reached.

The crucial difference to the BCS formalism in homogeneous infinite matter is that in our case the wave functions adapt themselves to the pairing field and to the Coulomb potential, whereas in the case of homogeneous infinite matter the wave functions always stay plane waves, and the U and V factors are just coefficients multiplying them.

¹ In uniform infinite matter it can be shown [5] that for the energetically favored solution the arbitrary orientation in color can be chosen in such a way that only the diagonal condensates with $A = A'$ are non-zero.

C. Determination of chemical potentials and bag radius

In Section IIB we described how the HFB equations are solved for given values of the chemical potentials μ_{fc} and of the bag radius R . However, in reality, only one quantity is given, namely the baryon number A . Even the fractions of different quark flavors cannot be fixed, unless one allows for β unstable strangelets. Let us now describe how we determine the chemical potentials μ_{fc} and the bag radius R for given baryon number A .

The first step consists in fixing the quark numbers, N_{fc} , for each flavor f and color c , and to adjust the chemical potentials μ_{fc} in order to obtain these quark numbers. Before we address the question how the nine quark numbers N_{fc} are determined, let us discuss the issue of the bag radius R . Until now, the radius was imposed from outside, but in reality the system will choose its radius such that it minimizes its total energy for given quark numbers N_{fc} . Within the bag model, the total energy is given by

$$E = E_q + BV, \quad (16)$$

where $V = 4\pi R^3/3$ is the volume of the bag. By E_q we denote the energy of the quarks inside the bag, including the interaction energy, which in our case comes from pairing and Coulomb interactions. It can be obtained from the solution of the HFB equations as follows [19]:

$$E_q = \int_{r < R} d^3r \sum_{\beta, \epsilon_\beta < 0} \left(U_\beta^\dagger(\mathbf{r})(\epsilon_\beta + \mu)U_\beta(\mathbf{r}) + \frac{1}{2} \left[\bar{U}_\beta(\mathbf{r})\Delta(r)V_\beta(\mathbf{r}) - U_\beta^\dagger(\mathbf{r})eQA_0(r)U_\beta(\mathbf{r}) \right] \right). \quad (17)$$

Minimizing the total energy E is of course completely equivalent to saying that the quark pressure in the bag is counterbalanced by the bag pressure B , i.e.,

$$\left. \frac{dE_q}{dV} \right|_N = -B. \quad (18)$$

This equation determines the radius of the strangelet for given bag pressure B , interaction strength H and quark numbers N_{fc} . In practice, however, we find it more convenient to minimize E rather than solve Eq. (18).

Let us now turn to the determination of the quark numbers. The nine quark numbers N_{fc} cannot be chosen arbitrarily, but they have to fulfil certain requirements. Imposing the total baryon number A and color neutrality, i.e., equal numbers of quarks for each color, we have to satisfy the constraint

$$\sum_f N_{fc} = A \quad \text{for all } c. \quad (19)$$

Of course, these three equations are not sufficient for determining all the nine quark numbers. In order to get

unique values for the N_{fc} , it is necessary to impose β stability, as we will describe now.

In an infinite homogeneous system the condition for β equilibrium gives just a relation between the chemical potentials²

$$\mu_{dc} = \mu_{sc} = \mu_{uc} + \mu_e \quad \text{for all } c. \quad (20)$$

In a small system this is slightly different. First, even if there are electrons (i.e., if the strangelet is charged), they are not localized inside the strangelet, but they form a large cloud like in ordinary atoms and hence their chemical potential μ_e is approximately equal to the electron mass and can be neglected. Without pairing, it has been estimated in Ref. [20] that this may be still the case for strangelets with charge $Z \lesssim 1000$, corresponding roughly to $A \lesssim 10^6$. The second difference to bulk matter comes from the fact that, due to the discrete levels, particle numbers are discontinuous functions of the chemical potentials. The term β equilibrium should now be replaced by β stability, which means that the system does not gain energy by performing a β decay, inverse β decay, or electron capture, i.e., transforming an up into a down or strange quark, or vice versa, accompanied by the corresponding leptons.

To achieve β stability, we therefore compare the energies of adjacent strangelets with the same total quark number per color, differing only in the number of up, down, and strange quarks, respectively, in order to find the configuration with the lowest total energy E . Of course, in the case of large particle numbers, the minimum-energy configuration fulfils approximately the condition (20).

D. Choice of the model parameters

Besides the quark masses, which we take as $m_u = m_d = 0$ and $m_s = 120$ MeV, our model contains three parameters: the bag constant B , the coupling constant of the pairing interaction, H , and the cutoff Λ which is necessary to avoid the divergence of the gap equation (9), see below Eq. (11). In fact, a change of the cutoff in reasonable limits can to very good approximation be compensated by a change of the coupling constant. We therefore choose rather arbitrarily $\Lambda = 600$ MeV and give instead of the dimensionful coupling constant H the dimensionless combination $H\Lambda^2$. So we are left with two parameters, B and $H\Lambda^2$.

We can get an idea of the value of the bag pressure by looking at the stability of bulk quark matter. Non-strange quark matter should be energetically less favored than normal hadronic matter, whereas SQM should be stable if for some baryon number $A > A_c$ strangelets

² Here we assume that neutrinos are not trapped, i.e., they can freely leave the system

TABLE I: Values of the bag constants for different values of the coupling constant H , resulting in color and electrically neutral SQM with electrons in β equilibrium with an energy per baryon of $E/A = 900$ MeV. The corresponding baryon densities ρ_B , electron densities ρ_e , and pairing gaps in infinite matter are also displayed.

$H\Lambda^2$	$B^{1/4}$ (MeV)	ρ_B (fm^{-3})	ρ_e (fm^{-3})	Δ_2 (MeV)	$\Delta_5 = \Delta_7$ (MeV)
0	152.03	0.329	7.3×10^{-6}	0	0
1.5	152.44	0.339	9.7×10^{-5}	27.7	0
1.75	153.97	0.367	0	35.1	34.5
2	156.26	0.395	0	50.6	49.7
2.25	159.46	0.427	0	67.2	66.0
2.5	163.46	0.463	0	84.6	83.1

become stable and consequently strange stars can exist. This means that we want the energy per baryon of SQM to be less than 931 MeV, the energy per baryon of the most stable nucleus, ^{56}Fe . On the other hand, the energy per baryon of non-strange quark matter should be larger than the nucleon mass. Without interaction the window for the values of the bag constant is then $148 \text{ MeV} < B^{1/4} < 157 \text{ MeV}$. These values change as a function of the interaction strength H . To better compare the results, we will readjust for each coupling strength the bag constant in order to get $E/A = 900$ MeV. The corresponding values are listed in Table I, together with other properties of infinite matter. Non-strange quark matter is unstable with these parameter values. Note that for the weakest non-vanishing coupling constant given in Table I, SQM is in the 2SC phase and not in the CFL phase. For the larger coupling constants, the CFL phase is preferred. Note that, due to the mass difference of light and strange quarks, the flavor $SU(3)$ symmetry is not exact and the gap Δ_2 is different from Δ_5 and Δ_7 . However, since the CFL phase is electrically neutral, and we have $m_u = m_d = 0$, the isospin $SU(2)$ symmetry in the up- and down-quark sector is exact and therefore $\Delta_5 = \Delta_7$.

III. RESULTS

A. Different types of solutions

We will first discuss the qualitatively different configurations we find. Let us start by discussing a small strangelet ($A = 108$, $Z = 24$) without any pairing interaction ($H\Lambda^2 = 0$). The mass number has been chosen such that the minimum-energy configuration is a closed-shell configuration. The quark numbers and other relevant information are listed in Table II. Due to the finite size of the bag, the energy per baryon ($E/A = 932.5$ MeV, including 1.0 MeV due to Coulomb) is much higher than that of color neutral infinite matter

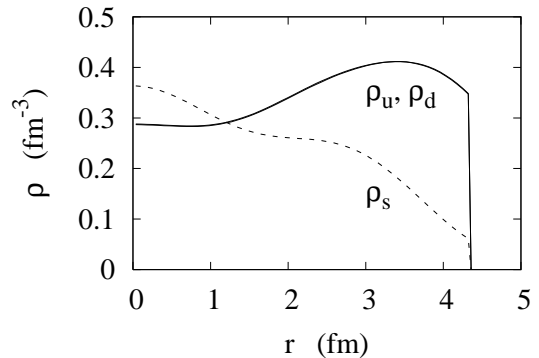


FIG. 1: Quark number density profiles of the strangelet $A = 108$, $Z = 24$ in the case of vanishing pairing interaction (free quarks in a bag) and $B^{1/4} = 152.03$ MeV.

with $\mu_{uc} = \mu_{dc} = \mu_{sc}^3$ ($E/A = 899.5$ MeV). This effect will be discussed in more detail in Section III C. The density profiles of light and strange quarks are shown in Fig. 1. As expected, due to the boundary condition, the strange-quark density is strongly suppressed at the surface, contrary to the densities of the light quarks. For comparison we mention that for the same value of the bag constant, the densities in color neutral infinite matter with $\mu_{uc} = \mu_{dc} = \mu_{sc}$ are: $\rho_u = \rho_d = 0.355 \text{ fm}^{-3}$, $\rho_s = 0.274 \text{ fm}^{-3}$. We see that not only the strange-quark density, but also the densities of the light quarks are quite different from these values and depend strongly on r because of the existence of discrete levels in the bag. Let us mention that, due to the Coulomb potential, the density profiles of up and down quarks are slightly different, but the difference is too small to be visible in Fig. 1.

Now we switch on the pairing interaction. In the case of $H\Lambda^2 = 1.5$, SQM is in the 2SC phase, i.e., only up and down quarks of two colors (red and green in our notation) are paired. This is also true in a finite strangelet. Therefore it is clear that the strange-quark density profile remains the same as without pairing. The oscillations of the densities of the light quarks, however, are much weaker now than in the case without pairing, since pairing washes out the occupation numbers. This can be seen in Fig. 2. In this 2SC-like solution, only one of the gaps, Δ_2 , is non-zero. Since Δ_2 involves only the wave functions of up and down quarks, which are not suppressed at the surface, it extends up to the surface of the bag, as shown in Fig. 3. As a function of r , it is almost constant and quite close to the corresponding value in infinite matter with $\mu_{uc} = \mu_{dc} = \mu_{sc}$, which is $\Delta_2 = 29.2$ MeV.

If we increase the coupling constant to $H\Lambda^2 = 1.75$, we

³ As discussed below Eq. (20), it is more appropriate to compare a small strangelet with this kind of matter rather than electrically neutral matter with electrons in β equilibrium.

TABLE II: Parameters and properties of the strangelets discussed in Section III A: B = bag constant, H = coupling constant of the pairing interaction, A = baryon number, Z = charge, N_{fc} = number of quarks of flavor f and color c , E/A = energy per baryon, R = radius of the bag, $\Delta_A(0)$ = value of the gap at $r = 0$.

$B^{1/4}$ (MeV)	$H\Lambda^2$ (MeV)	A	Z	$\begin{pmatrix} N_{ur} & N_{ug} & N_{ub} \\ N_{dr} & N_{dg} & N_{db} \\ N_{sr} & N_{sg} & N_{sb} \end{pmatrix}$	E/A (MeV)	R (fm)	$\Delta_2(0)$ (MeV)	$\Delta_5(0)$ (MeV)	$\Delta_7(0)$ (MeV)
152.03	0	108	24	$\begin{pmatrix} 44 & 44 & 44 \\ 44 & 44 & 44 \\ 20 & 20 & 20 \end{pmatrix}$	932.5	4.36	0	0	0
152.44	1.5	108	24	$\begin{pmatrix} 44 & 44 & 44 \\ 44 & 44 & 44 \\ 20 & 20 & 20 \end{pmatrix}$	930.7	4.31	32.9	0	0
153.97	1.75	108	24	$\begin{pmatrix} 44 & 44 & 44 \\ 44 & 44 & 44 \\ 20 & 20 & 20 \end{pmatrix}$	934.0	4.24	49.5	0	0
153.97	1.75	108	10	$\begin{pmatrix} 38 & 39 & 41 \\ 39 & 38 & 41 \\ 31 & 31 & 26 \end{pmatrix}$	934.8	4.21	41.6	24.9	24.9
153.97	1.75	108	0	$\begin{pmatrix} 38 & 35 & 35 \\ 35 & 38 & 35 \\ 35 & 35 & 38 \end{pmatrix}$	934.8	4.17	33.9	37.0	36.9

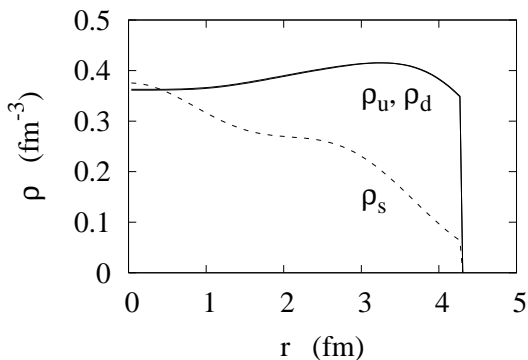


FIG. 2: Quark number density profiles of the strangelet $A = 108$, $Z = 24$ in the case of $H\Lambda^2 = 1.5$ and $B^{1/4} = 152.44$ MeV.

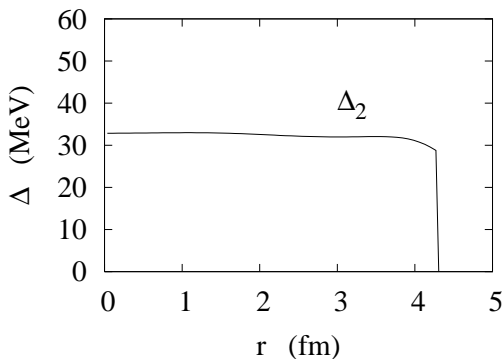


FIG. 3: Gap $\Delta_2(r)$ of the strangelet $A = 108$, $Z = 24$ in the case of $H\Lambda^2 = 1.5$ and $B^{1/4} = 152.44$ MeV.

obtain three qualitatively different solutions which have comparable energies. The most stable one is still of the 2SC type, although in infinite matter the CFL phase is preferred. In this case, the strangelet still has $Z = 24$ and the density profiles are almost identical to those shown in Fig. 2. The main difference is that now the value of

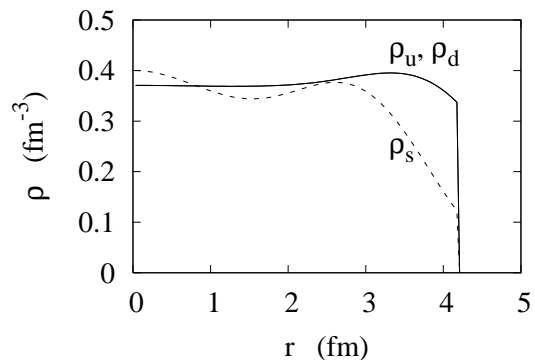


FIG. 4: Density profiles of the strangelet $A = 108$, $Z = 10$ in the case of $H\Lambda^2 = 1.75$ and $B^{1/4} = 153.97$ MeV.

the gap is larger.

In the two other solutions, also strange quarks participate in pairing ($\Delta_5 \approx \Delta_7 \neq 0$ – note that Δ_5 and Δ_7 are not exactly equal because the isospin symmetry is broken by the Coulomb interaction). These two solutions have charge $Z = 10$ and $Z = 0$, respectively. Let us first discuss the case $Z = 10$. In this case, there are a couple of up and down quarks which remain unpaired. The wave function of the unpaired level is mainly localized near the surface of the bag, as can be seen in Fig. 4, where the density profiles are shown. In the inner part, the densities of up, down, and strange quarks are almost equal, while near the surface, where the strange-quark density is suppressed due to the boundary condition, there is an excess of up and down quarks. This excess is due to the unpaired quarks. The fact that one level of up and down quarks (in the present case the $1g_{9/2}$ level, i.e., the lowest level with $j = 9/2$, $\kappa = -5$ in the notation of Appendix A) does not participate in pairing means that the occupation number of this level is equal to 1. At the same time, the corresponding level of the strange quarks has an occupation number equal to 0. In a certain sense this situation is analogous to the “breached pairing” phase

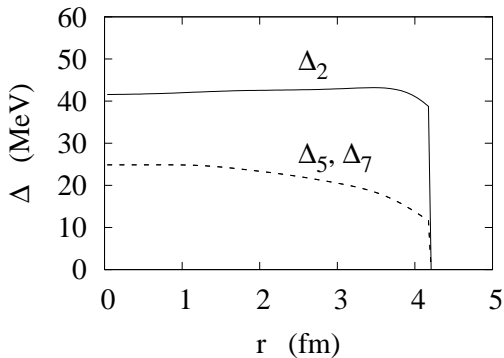


FIG. 5: Gaps Δ_A as functions of r for the strangelet $A = 108$, $Z = 10$ in the case of $H\Lambda^2 = 1.75$ and $B^{1/4} = 153.97$ MeV.

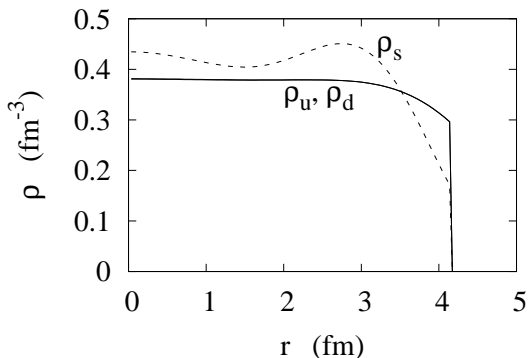


FIG. 6: Density profiles of the strangelet $A = 108$, $Z = 0$ in the case of $H\Lambda^2 = 1.75$ and $B^{1/4} = 153.97$ MeV.

of infinite matter [21]. The charge Z is equal to the degeneracy $2j + 1$ of the unpaired level. The gaps Δ_A as functions of r corresponding to this solution are displayed in Fig. 5.

In the third solution, all quarks are paired. As a consequence, the numbers of up, down, and strange quarks are equal, and the total charge is $Z = 0$. This is analogous to the CFL phase in the infinite system. Since the strange-quark density is suppressed near the surface, but the number of strange quarks is equal to that of up and down quarks, it is clear that the strange-quark density must be larger than the up- and down-quark densities in some other part of the system. This is indeed the case, as can be seen in Fig. 6. We also see that the excess of the light-quark densities over the strange-quark density is reduced as compared with the case $Z = 10$ discussed above (cf. Fig. 4). We will discuss the charge-density distribution in detail in Section III B. The gaps, shown in Fig. 7, are much closer to the gaps in infinite matter (cf. Table I) than in the case $Z = 10$.

For the larger values of the coupling constant we considered ($H\Lambda^2 = 2, 2.25, 2.5$), it is always the CFL-type solution ($Z = 0$) which has the lowest energy. We do not show any figures because in all these cases the results are analogous to those shown in Figs. 6 and 7 (just the va-

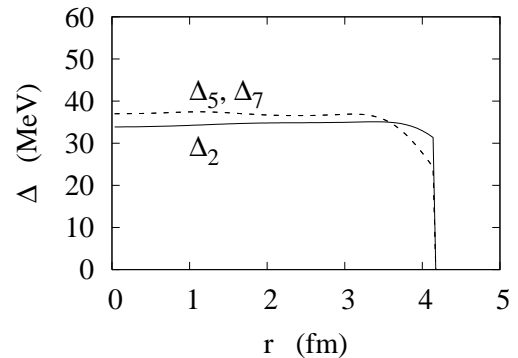


FIG. 7: Gaps Δ_A as functions of r for the strangelet $A = 108$, $Z = 0$ in the case of $H\Lambda^2 = 1.75$ and $B^{1/4} = 153.97$ MeV.

lues of the gaps change, they are close to those given in Table I for infinite matter).

It should be mentioned that the fully paired solutions with $Z = 0$ are very robust as soon as the coupling constant is sufficiently large, i.e., we find this type of solution for arbitrary numbers of quarks⁴. This solution is in contrast to previous findings (see, e.g., Ref. [15]), where it was supposed that the CFL matter should be neutral in the bulk with just a thin positively charged surface layer with an excess of up and down quarks because of the boundary condition. In fact, this idea corresponds roughly to our solution with unpaired up and down quarks near the surface. This solution is, however, very fragile and exists only for certain values of parameters and mass numbers, since it requires the existence of a suitable level of light and strange quarks near the respective Fermi surfaces which can serve as unpaired level.

B. Charge density distribution

We have seen in Section III A that in all cases except the 2SC phase, pairing drastically reduces the total charge Z . Because of surface effects, the local charge density does, however, not vanish, even within the CFL-type solution which has $Z = 0$. Due to the suppression of the strange-quark wave function at the surface, a positively charged surface layer remains with an extension of ~ 1 fm, as has already been pointed out in Ref. [15].

Within the configuration with some unpaired light quarks at the surface, the total charge of the strangelet results from this positive surface charge, the interior of the strangelet has almost zero charge density. The total charge is here reduced compared with a strangelet without pairing, for example the $A = 108$ strangelet has

⁴ If the number of quarks is odd, it is impossible to pair all quarks and one or several state(s) should be “blocked” by the unpaired quark(s). At present, we have not included this effect in our calculation, and we restrict ourselves to even quark numbers

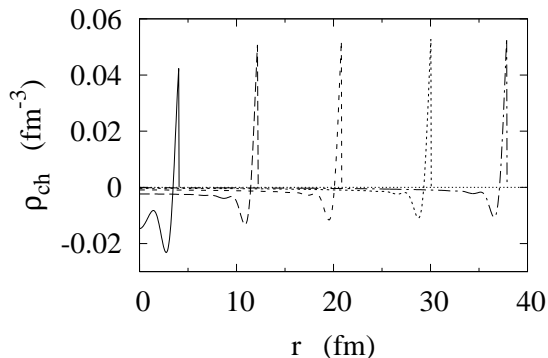


FIG. 8: Charge density profiles of the fully paired ($H\Lambda^2 = 2$) strangelets $A = 108, 3000, 15000, 45000,$ and 90000 (from left to right).

$Z = 10$ within this paired configuration, whereas the corresponding unpaired strangelet has $Z = 24$. A systematic study of the total charge of strangelets in this configuration will not be discussed here since this configuration is rather fragile with respect to the details of the single-particle spectra and thus difficult to realize for many different particle numbers.

Let us therefore concentrate on the CFL-type solution, which exists for arbitrary particle numbers. We consider different mass numbers A from $A = 108$ to $A = 90000$, for one particular value of the coupling constant, $H\Lambda^2 = 2$. In order to reduce the considerable numerical effort, we use for the large strangelets (starting from $A = 15000$) the condition (20) with $\mu_e = 0$ (as a consequence, the quark numbers for each flavor and color are not integers) instead of looking for the true energy minimum with respect to β decay. In addition, we do not minimize the energy with respect to the radius, but we simply estimate the volume of the bag by dividing the mass number A by the baryon density $\rho_{B \text{ bulk}}$ of infinite matter. These two approximations are very accurate for such large strangelets. Already in the case of $A = 3000$, the quark numbers and the radius are very well reproduced within these approximations: the full minimization results in quark numbers $N_{ur} = N_{dg} = N_{sb} = 1052$, $N_{ug} = N_{dr} = N_{ub} = N_{sr} = N_{db} = N_{sg} = 974$, and a radius $R = 12.23$ fm, while the approximations lead to $N_{ur} = 1051.8$, $N_{dg} = 1051.7$, $N_{sb} = 1051.1$, $N_{ug} = N_{dr} = 973.8$, $N_{ub} = N_{sr} = 974.4$, $N_{db} = N_{sg} = 974.5$, and $R = 12.19$ fm. Our results for the charge densities for $A = 108, 3000, 15000, 45000,$ and 90000 are shown in Fig. 8.

Since all quarks are paired, we have equal numbers of up, down, and strange quarks such that the total charge of these strangelets is zero. The positive surface charge is mostly compensated by an excess of negative charge concentrated at around 1-3 fm below the surface. We stress that this concentration of negative charge in a thin layer is a consequence of pairing and the effect persists if Coulomb interaction is switched off. In fact,

since also the strange quarks are paired, the “missing” strange-quark density at the surface must be compensated by an “overshooting” of the strange-quark density within a distance corresponding to the size of the Cooper pairs, i.e., the coherence length ξ . Due to the strong gap, the coherence length is very small: Using the estimate $\xi \sim 1/(\pi\Delta)$, one finds that it is of the same order as the Fermi wavelength and, strictly speaking, one might therefore question that mean-field results are quantitatively correct [22]. The smallness of ξ explains why the compensation of the negative surface charge is mostly concentrated in such a thin layer at a small distance from the surface.

Below this strongly negatively charged layer, the charge density stays negative but much smaller. Due to Coulomb interaction, which tries to push the charge towards the surface, this negative charge density decreases with increasing distance from the surface, especially for large strangelets. Actually, if Coulomb interaction is switched off, the remaining charge is distributed more or less homogeneously over the whole volume.

The behaviour of the charge density far away from the surface in the presence of Coulomb interaction can easily be interpreted in terms of Debye screening (similar considerations can be found in Ref. [23] for the case of hadron-quark mixed phases): We know that in a uniform medium with Debye screening the Laplace equation for the Coulomb potential is replaced by

$$\left(\nabla^2 - \frac{1}{\lambda^2}\right)A_0 = 0, \quad (21)$$

where λ is the screening length, which can be obtained from the limit $\Pi^{00}(q^0 = 0, \mathbf{q} \rightarrow 0)$, where $\Pi^{\mu\nu}(q)$ is the polarization tensor in the uniform system. This is equivalent to the expression [23]

$$\frac{1}{\lambda^2} = 4\pi e^2 \sum_{fc} Q_f \frac{\partial \rho_{ch}}{\partial \mu_{fc}}. \quad (22)$$

Computing numerically this derivative within our model for the case of bulk CFL matter with $B = 156.26$ MeV and $H\Lambda^2 = 2$, we obtain $\lambda = 7.74$ fm.

Taking the Laplacian of Eq. (21), we see that the charge density obeys the analogous equation

$$\left(\nabla^2 - \frac{1}{\lambda^2}\right)\rho_{ch} = 0. \quad (23)$$

In the case of half-infinite matter with a surface at $z = 0$, the solution of this equation shows that the charge density goes to zero as $\rho_{ch} \propto \exp(z/\lambda)$ if one goes away from the surface ($z \rightarrow -\infty$). In the case of a sphere, the corresponding solution reads

$$\rho_{ch} \propto \frac{\sinh(r/\lambda)}{r/\lambda}. \quad (24)$$

Far away from the surface, the charge densities which we obtain are very well described by Eq. (24). To show

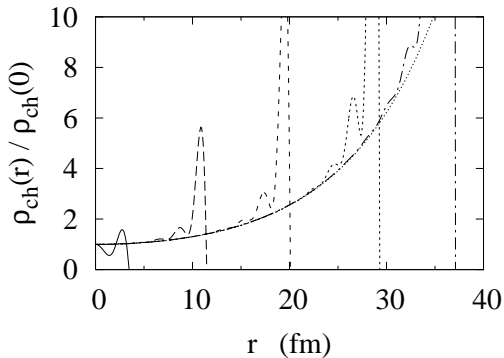


FIG. 9: Zoom into the part of Fig. 8 where the charge density behaves as given by Eq. (24). For a better visibility, the charge densities have been divided by their respective values at $r = 0$. The thin dotted curve corresponds to Eq. (24) with $\lambda = 7.74$ fm.

this, we display in Fig. 9 the same charge densities as in Fig. 8, but divided by their value at $r = 0$. Far away from the surface, all curves follow exactly Eq. (24) with the value $\lambda = 7.74$ fm calculated for bulk CFL matter. Near the surface, i.e., at distances which are of the order of a couple of Fermi wavelengths, there are strong deviations from this behavior due to Friedel-type oscillations [24]. This is because Eq. (21) is not exact, but it is only valid in a uniform medium and in the long-wavelength limit.

It is interesting to notice that the value of the Debye screening length we obtain is in reasonable agreement with the photon Debye mass calculated from perturbative QCD, which reads, for the CFL phase, $m_{D,\gamma\gamma}^2 = 1/\lambda^2 = 4 \frac{21-8\ln 2}{54} e^2 N_f \mu^2 / (6\pi^2)$ [25] ($m_{D,\gamma\gamma}$ denotes the Debye mass without gluon-photon mixing, see below). For typical values of the chemical potential this gives $\lambda \sim 10$ fm.

In principle, in color superconducting phases, the photon can mix with one of the gluons. In the CFL phase, in bulk matter, one linear combination of photon and gluon stays massless. This means that at large distances $d \gg \xi$, the Debye screening for the “rotated” photon [26, 27] does not work, since the Cooper pairs are neutral with respect to the rotated charge \tilde{Q} . Within the simple model we use for the moment, there are no gluons, such that the mixing cannot be studied. It could be taken into account, as mentioned at the end of Section II, by including the gluons in the same way as the photon, i.e., on the Hartree level. We expect that if we included the gluons in this way, we would find an even faster decrease of the charge if we go away from the surface, since in addition to the electromagnetic force we would have the color forces, which try to push the color charges to the surface, and in the CFL phase color neutrality goes hand in hand with electrical neutrality. Therefore, this is not in contradiction with the fact that the rotated photon is massless, but it is just a consequence of the fact that the combination of photon and gluon which is orthogonal to

TABLE III: Fitted liquid-drop parameters for the CFL-type neutral strangelets ($Z = 0$). The surface tension σ corresponding to the fitted value of a_S is also given.

$B^{1/4}$ (MeV)	$H\Lambda^2$ (MeV)	a_S (MeV)	a_C (MeV)	σ (MeV/fm ²)
156.26	2	107	289	11.9
159.46	2.25	109	297	12.8
163.46	2.5	112	306	13.9

the rotated photon is massive (in fact, it is even heavier than the other gluons [27]). This means that in a large object, like a strange star, all the negative charge will be concentrated within a layer of a thickness of at most a few tens of fm below the surface. However, before drawing any firm conclusion, one should study this problem in more detail. This will be left for future work.

C. Liquid-drop type expansion

The advantage of the present approach is that finite size effects are correctly implemented. For large numbers of particles, this becomes, however, rather cumbersome and asymptotic expansions such as a liquid-drop type approach can be very useful. We will discuss here the determination of the parameters, such as the surface tension, of a liquid-drop type formula for the energy per baryon as a function of the baryon number A , including a surface and a curvature term,

$$\frac{E}{A} = \left(\frac{E}{A} \right)_{bulk} + \frac{a_S}{A^{1/3}} + \frac{a_C}{A^{2/3}}, \quad (25)$$

from our results. As in Section III B, we will restrict our discussion to the CFL-type solutions with $Z = 0$, such that we do not need to include a Coulomb term $\propto Z/A^{1/3}$.

As explained after Eq. (20), $(E/A)_{bulk}$ should be the energy per baryon of infinite matter with $\mu_e = 0$ rather than that of β stable infinite matter. However, since we consider only the CFL-type solution, this distinction is irrelevant. Hence, for our chosen parameter sets, we have $(E/A)_{bulk} = 900$ MeV. Since for the neutral strangelets the Coulomb interaction has only a negligible effect on the total energies (for example, in the case of the strangelets considered in Section III B, the Coulomb interaction changes the total energy per baryon by less than 5 keV) it will be neglected here in order to reduce the numerical effort. The result of the fitted coefficients a_S and a_C for the different parameter sets are listed in Table III. As an example, in order to show the accuracy of the asymptotic expansion, we display in Fig. 10 some results for the energy per baryon together with the liquid-drop formula, Eq. (25). The dashed line corresponds to the liquid-drop formula without the curvature term ($a_C = 0$). From this figure it becomes clear that

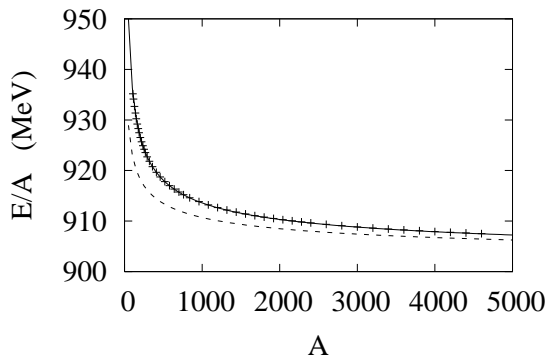


FIG. 10: Energy per baryon as a function of baryon number for $H\Lambda^2 = 2$ and $B^{1/4} = 156.26$ MeV. The exact results are indicated by the crosses, the fitted liquid-drop formula by the solid line. The dashed line corresponds to the liquid-drop formula without the curvature term.

the liquid-drop formula with curvature term works extremely well, much better than in the case without pairing [28]. The reason is that shell effects are completely washed out because, contrary to the situation in ordinary nuclei, the pairing gap is much larger than the spacing between neighboring shells. Another interesting observation is that the curvature term is very important, even for rather large mass numbers A .

The coefficient a_S is closely related to a very interesting quantity, namely the surface tension. As explained in Ref. [29], the surface tension is obtained as

$$\sigma = \frac{E_S}{4\pi R_0^2}, \quad (26)$$

where

$$E_S = E - A \left(\frac{E}{A} \right)_{bulk} \quad (27)$$

is the energy excess due to the surface and R_0 is an effective radius defined by

$$A = \rho_{B\ bulk} \frac{4\pi R_0^3}{3}, \quad (28)$$

which is actually very close to R for not too small strangelets. On the one hand, using the liquid-drop formula (25) for E in Eq. (26), one would obtain a surface tension which depends on A because of the curvature term. Therefore it is clear that one has to use Eq. (26) in the limit $A \rightarrow \infty$, where the curvature term vanishes, i.e.,

$$\sigma = \frac{a_S \rho_{B\ bulk}^{2/3}}{(36\pi)^{1/3}}. \quad (29)$$

The corresponding numbers are given in the last column of Table III. They are of the same order of magnitude as the estimate $\sigma \sim (70 \text{ MeV})^3 = 8.8 \text{ MeV}/\text{fm}^2$ for SQM

without color superconductivity [20]. On the other hand, the fact that the curvature term is very strong implies that the knowledge of the surface tension alone might not be sufficient in order to determine, e.g., the possibility of mixed phases, the size of droplets, etc.

Before we conclude, let us comment on the physical meaning of the surface tension we obtain. In the MIT bag model, it is supposed that the energy needed to create a bag with volume V is simply given by BV . In principle one could imagine that there is an explicit dependence of the bag energy on, e.g., the surface or the curvature of the bag boundary. In Ref. [20], this contribution to the surface tension was called “intrinsic surface tension”, σ_I , and it was argued that it should be small. What we calculate here is the “dynamical surface tension”, σ_D , which has its origin in the change of the level density of the quarks inside the bag as a function of the bag geometry.

IV. SUMMARY

In this paper we have investigated finite lumps of color superconducting SQM. To that end we have treated the MIT bag model, supplemented with a pairing interaction, in the framework of HFB theory. This allows us to correctly include finite size effects for pairing, too. The calculation is numerically rather involved, since in addition to solving self-consistently the HFB equations, we have to determine the bag radius and the fractions of the different quark species by minimizing the total energy of the system.

As expected from previous MIT bag-model studies, we find a suppression of the strange-quark densities at the surface, resulting in a positive surface charge. Our main result is that, in spite of this surface charge, the total charge of the CFL type solution is zero due to pairing, as in bulk matter. Most of the positive surface charge is compensated in a negatively charged layer situated at about 1-3 fm below the surface. The origin of this concentration of the negative charge is pairing: Since all quarks are paired, the positive surface charge must be compensated on a length scale corresponding to the coherence length. The remaining negative charge, which is necessary to compensate all of the positive surface charge, is situated below this layer. With increasing distance from the surface, the charge density decreases on a length scale of ~ 8 fm, corresponding to the Debye screening length. This number will probably be strongly decreased if the gluons are included in a perturbative way similar to the photon. In any case, in the biggest part of a large object, such as a strange star, one finds vanishing charge density if one goes more than a few tens of fm away from the surface. It remains to be investigated in which way our results change the traditional picture of the surface of a strange star and the detectability of smaller strangelets in current experiments such as AMS-02 or LSSS [30].

We have also compared our results for the energy per

baryon of finite strangelets with a liquid-drop like formula. We obtain a surface tension of the order of 12-14 MeV, in reasonable agreement with previous studies where color superconductivity was not considered, and a strong curvature term which is crucial to reproduce the correct energies up to baryon numbers of several thousands. An interesting result is that, in the presence of color superconductivity, the liquid-drop formula describes very accurately the total energies even for $A \lesssim 100$, at least for strangelets with even baryon number. The reason is that, since the gap Δ is much larger than the spacing between the energy levels, shell effects are strongly suppressed.

Acknowledgements

We thank Michael Buballa for useful discussions and for the critical reading of the first version of this manuscript.

APPENDIX A: SPINORS IN A SPHERICAL CAVITY

In this appendix we recall basic properties of free Dirac spinors in a spherical cavity (see, e.g., Ref. [18]). They can be written as

$$\psi_{ffj\kappa mn}(\mathbf{r}) = \begin{pmatrix} g_{ffj\kappa n}(r) \mathcal{Y}_{jl}^m(\Omega) \\ i f_{ffj\kappa n}(r) \mathcal{Y}_{j'l'}^m(\Omega) \end{pmatrix}, \quad (\text{A1})$$

where \mathcal{Y} are spinor spherical harmonics [31]. We have the following relations between the angular momentum quantum numbers

$$\begin{aligned} \kappa = j + \frac{1}{2} &\rightarrow l = j + \frac{1}{2}, \quad l' = j - \frac{1}{2} \\ \kappa = -(j + \frac{1}{2}) &\rightarrow l = j - \frac{1}{2}, \quad l' = j + \frac{1}{2}. \end{aligned} \quad (\text{A2})$$

For the solutions of the free Dirac equation, the functions f and g are given as follows in terms of the spherical Bessel functions ($\xi_{ffj\kappa n} = \sqrt{p_{ffj\kappa n}^2 + m_f^2}$)

$$\begin{aligned} g_{ffj\kappa n}(r) &= C_{ffj\kappa n} j_l(p_{ffj\kappa n} r) \\ f_{ffj\kappa n}(r) &= C_{ffj\kappa n} \text{sgn}(\kappa n) \sqrt{\frac{\xi_{ffj\kappa n} - m_f}{\xi_{ffj\kappa n} + m_f}} j_{l'}(p_{ffj\kappa n} r), \end{aligned} \quad (\text{A3})$$

where the $C_{ffj\kappa n}$ are normalisation coefficients which can be determined from the normalization

$$\int_0^R dr r^2 \int d\Omega \psi^\dagger(\mathbf{r}) \psi(\mathbf{r}) = 1. \quad (\text{A4})$$

The momenta $p_{ffj\kappa n}$ are obtained from the boundary condition. The boundary condition of the MIT bag model,

Eq. (1), translates into the following equation

$$f_{ffj\kappa n}(R) = -g_{ffj\kappa n}(R), \quad (\text{A5})$$

or, explicitly,

$$j_l(p_{ffj\kappa n} R) = \text{sgn}(\kappa n) \sqrt{\frac{\xi_{ffj\kappa n} - m_f}{\xi_{ffj\kappa n} + m_f}} j_{l'}(p_{ffj\kappa n} R), \quad (\text{A6})$$

where we number by $n > 0$ the positive-energy (particle) states and by $n < 0$ the negative-energy (antiparticle) states. In practice, we will keep only the states with positive eigenvalues and neglect the antiparticle contributions. The latter can approximately be absorbed into a redefinition of the coupling constant.

APPENDIX B: HFB EQUATIONS

In this appendix we will give some more details about the HFB equations. Their derivation is analogous to the derivation of the Dirac-Hartree-Bogoliubov equations in finite nuclei, which is given in Ref. [19].

The HFB equations are derived from the Lagrangian by minimizing the energy in the mean field approximation, i.e., linearizing the interaction under the assumption of nonzero expectation values for the condensates $s_{AA'}(x)$, Eq. (7). Due to the inhomogeneities of a finite system, the Green's functions become nondiagonal in momentum. In the stationary case, it is convenient to work in \mathbf{r} space for the spatial coordinates but to perform the Fourier transformation for the time variable. Then the Green's functions,

$$S(x, y) = -i \langle T(\Psi(x) \bar{\Psi}(y)) \rangle, \quad (\text{B1})$$

with

$$\Psi(x) = \begin{pmatrix} \psi(x) \\ \psi_T(x) \end{pmatrix} \quad (\text{B2})$$

take the following general form in Nambu-Gorkov space:

$$\begin{aligned} S(\mathbf{r}, \mathbf{r}'; \omega) &= \begin{pmatrix} G(\mathbf{r}, \mathbf{r}'; \omega) & F(\mathbf{r}, \mathbf{r}'; \omega) \\ \tilde{F}(\mathbf{r}, \mathbf{r}'; \omega) & \tilde{G}(\mathbf{r}, \mathbf{r}'; \omega) \end{pmatrix} \\ &= \sum_{\alpha(\epsilon_\alpha > 0)} \begin{pmatrix} U_\alpha(\mathbf{r}) \\ V_\alpha(\mathbf{r}) \end{pmatrix} \frac{1}{\omega - \epsilon_\alpha + i\eta} (\bar{U}_\alpha(\mathbf{r}'), \bar{V}_\alpha(\mathbf{r}')) \\ &+ \sum_{\beta(\epsilon_\beta < 0)} \begin{pmatrix} U_\beta(\mathbf{r}) \\ V_\beta(\mathbf{r}) \end{pmatrix} \frac{1}{\omega + \epsilon_\beta - i\eta} (\bar{U}_\beta(\mathbf{r}'), \bar{V}_\beta(\mathbf{r}')), \end{aligned} \quad (\text{B3})$$

where G, \tilde{G} and F, \tilde{F} are normal and anomalous Green's functions, respectively. The spinors $U_{\alpha,\beta}$ and $V_{\alpha,\beta}$ correspond to the particle- and hole-like components, respectively.

The energy in mean-field approximation can now be written as [19]

$$E_q = \int d^3x \left(i \text{Tr}[(i\boldsymbol{\gamma} \cdot \boldsymbol{\nabla} - m)G(x, x^+)] - \frac{i}{2} \int d^4y \text{Tr}[\Sigma(x, y)G(y, x^+) - \Delta(x, y)\tilde{F}(y, x^+)] \right), \quad (\text{B4})$$

where the derivative in the first term acts only on x and not on x^+ , and x^+ means the four vector $(x^0 + t, \mathbf{x})$ in the limit $t \rightarrow 0^+$. In our case, the normal and anomalous self-energies Σ and Δ are local and time-independent: $\Sigma(x, y) = eQA_0(\mathbf{x})\gamma^0\delta(x-y)$ and $\Delta(x, y) = \Delta(\mathbf{x})\delta(x-y)$, and Eq. (B4) can be reduced to Eq. (17).

As mentioned in Section II B, the expectation values (like condensates, densities, etc.) which are needed for calculating self-consistently the self-energy Σ and the pairing field Δ can be expressed in terms of the U and V functions. To that end, it is sufficient to express them in terms of the Green's functions, e.g.

$$s_{AA'} = -\langle \bar{\psi}_T(x)\tau_A\lambda_{A'}\psi(x) \rangle = i \text{Tr} F(x, x^+)\tau_A\lambda_A, \quad (\text{B5})$$

which leads to Eq. (9).

By minimizing the total energy with respect to the U and V functions, one obtains the HFB equations, [see Eq. (5)]:

$$\mathcal{H}W_\alpha = \epsilon_\alpha W_\alpha, \quad (\text{B6})$$

with $W_\alpha = (U_\alpha, V_\alpha)^T$ and \mathcal{H} being the matrix on the left-hand side of Eq. (5).

For homogeneous infinite systems the matrix elements of \mathcal{H} are diagonal in momentum space and solutions to the HFB equations are known for many cases. For finite systems, in general, these equations are solved numerically by diagonalizing the matrix \mathcal{H} in some conveniently chosen basis. Here, we are working in the basis which diagonalizes the Dirac hamiltonian (i.e., h_{fc} without the Coulomb potential), see Appendix A, and the eigenvectors $U_\alpha(\mathbf{r})$ and $V_\alpha(\mathbf{r})$ are developed within this basis.

The matrix elements of the pairing fields $\Delta_A(r)$ and of the Coulomb field $A_0(r)$ are computed in the usual way. For illustration, we give here the explicit expression for the matrix elements of $\Delta_2(r)$, which connects up and down quarks, in the basis described in Appendix A:

$$\begin{aligned} (\Delta_2)_{j\kappa nn'} &= \int_{r < R} d^3r \psi_{uj\kappa mn}^\dagger(\mathbf{r})\Delta_2(r)\psi_{dj\kappa mn'}(\mathbf{r}) \\ &= \int_0^R dr r^2 \Delta_2(r)(g_{uj\kappa n}(r)g_{dj\kappa n'}(r) \\ &\quad + f_{uj\kappa n}(r)f_{dj\kappa n'}(r)). \end{aligned} \quad (\text{B7})$$

Note that, due to spherical symmetry, all matrices are diagonal in j and κ and proportional to the unit matrix with respect to m .

In spite of the spherical symmetry, the matrix to be diagonalized is still huge, limiting the baryon number which can be calculated with reasonable computational effort. It is therefore important to reduce the size of the actual matrix to be diagonalized. By means of an orthogonal transformation

$$\tilde{\mathcal{H}} = S\mathcal{H}S^T, \quad \tilde{W} = SW, \quad SS^T = 1 \quad (\text{B8})$$

in color, flavor, and Nambu-Gorkov space, the matrix can actually be block-diagonalized (see, e.g., Ref. [32]) containing seven blocks. Six of them, $\tilde{\mathcal{H}}_{B,\dots,G}$, are 2×2 matrices in Nambu-Gorkov space, describing mutual pairing of two particles, such as, e.g., red down quarks (dr) with green up quarks (ug):

$$\tilde{\mathcal{H}}_B = \begin{pmatrix} h_{ug} & \Delta_2 \\ \Delta_2 & -h_{dr} \end{pmatrix}, \quad (\text{B9})$$

where h_{fc} is the single particle Hamiltonian for flavor f and color c . The second and third 2×2 blocks are

$$\tilde{\mathcal{H}}_C = \begin{pmatrix} h_{ub} & \Delta_5 \\ \Delta_5 & -h_{sr} \end{pmatrix}, \quad \tilde{\mathcal{H}}_D = \begin{pmatrix} h_{db} & \Delta_7 \\ \Delta_7 & -h_{sg} \end{pmatrix}. \quad (\text{B10})$$

Since we have in addition the pairwise relations $\tilde{\mathcal{H}}_{E,F,G} = -\tilde{\mathcal{H}}_{B,C,D}$, only three of the six 2×2 blocks have to be diagonalized in practice. The seventh block, $\tilde{\mathcal{H}}_A$, is 6×6 in Nambu-Gorkov space and describes pairing between red up, green down and blue strange quarks

$$\tilde{\mathcal{H}}_A = \begin{pmatrix} h_{ur} & 0 & 0 & 0 & \Delta_2 & \Delta_5 \\ 0 & h_{dg} & 0 & \Delta_2 & 0 & \Delta_7 \\ 0 & 0 & h_{sb} & \Delta_5 & \Delta_7 & 0 \\ 0 & \Delta_2 & \Delta_5 & -h_{ur} & 0 & 0 \\ \Delta_2 & 0 & \Delta_7 & 0 & -h_{dg} & 0 \\ \Delta_5 & \Delta_7 & 0 & 0 & 0 & -h_{sb} \end{pmatrix}. \quad (\text{B11})$$

APPENDIX C: CUTOFF FOR THE GAP EQUATION

As mentioned in Section II B, the divergent gap equation is regularized with the help of a smooth cutoff function

$$f(p/\Lambda) = \frac{1}{1 + c_1 \exp(c_2 a(p/\Lambda - 1))}, \quad (\text{C1})$$

where $c_1 = \sqrt{2} - 1$, $c_2 = 1/(4 - 2\sqrt{2})$, and $a = 22.58$ have been chosen such that $f^2(p/\Lambda)$ approximates the cutoff function $g(p/\Lambda)$ used in Ref. [33], but our function has the advantage to fall off more rapidly at very high momenta, which allows us to truncate the basis at a lower energy.

This function is used as a form factor multiplying each of the four legs of the four-point vertex. In practice,

this means that the form factor is used in two places: First, when calculating $s_{AA}(r)$, and second, when calculating the matrix elements of $\Delta_A(r)$ in the basis of the spinors defined in Appendix A. It should be noted that the diagonalization of the HFB matrix does not directly provide us with the eigenfunctions $U_\alpha(\mathbf{r})$ and $V_\alpha(\mathbf{r})$, but with their respective expansion coefficients in the basis

of the spinors defined in Appendix A. When calculating $s_{AA}(r)$ according to Eq. (9), the coefficients have to be multiplied with the corresponding basis functions, and in this step the factor $f(p_{fj\kappa n}/\Lambda)$ is attached to each basis function. Second, when calculating the matrix elements of the gap Δ_A , we again attach a factor $f(p_{fj\kappa n}/\Lambda)$ to each basis function.

-
- [1] J.C. Collins and M.J. Perry, Phys. Rev. Lett. **34**, 1353 (1975); B. Barrois, Nucl. Phys. **B129**, 390 (1977); S.C. Frautschi, Asymptotic freedom and color superconductivity in dense quark matter, in: Proc. of the Workshop on Hadronic Matter at Extreme Energy Density, N. Cabibbo (ed.), Erice 1978; D. Bailin and A. Love, Phys. Rep. **107**, 325 (1984).
- [2] M.G. Alford, K. Rajagopal, and F. Wilczek, Phys. Lett. B **422**, 247 (1998).
- [3] R. Rapp, T. Schäfer, E.V. Shuryak, and M. Velkovsky, Phys. Rev. Lett. **81**, 53 (1998).
- [4] K. Rajagopal and F. Wilczek, in: M. Shifman (Editor), *At the Frontier of Particle Physics, Handbook of QCD, Boris Ioffe Festschrift*, vol. 3, p. 2061 (World Scientific, Singapore 2001) [hep-ph/0011333]; M. Alford, Ann. Rev. Nucl. Part. Sci. **51**, 131 (2001); T. Schäfer, hep-ph/0304281; D.H. Rischke, Prog. Part. Nucl. Phys. **52**, 197 (2004); M. Buballa, Phys. Rep. **407**, 205 (2005); H.-C. Ren, hep-ph/0404074; M. Huang, Int. J. Mod. Phys. E **14**, 675 (2005); I. A. Shovkovy, Found. Phys. **35**, 1309 (2005).
- [5] M.G. Alford, K. Rajagopal, and F. Wilczek, Nucl. Phys. B **537**, 443 (1999).
- [6] I.A. Shovkovy and L.C.R. Wijewardhana, Phys. Lett. B **470**, 189 (1999); T. Schäfer, Nucl. Phys. B **575**, 269 (2000); N.J. Evans, J. Hormuzdiar, S.D.H. Hsu, and M. Schwetz, Nucl. Phys. B **581**, 391 (2000).
- [7] A.R. Bodmer, Phys. Rev. D **4**, 1601 (1971); E. Witten, Phys. Rev. D **30**, 272 (1984).
- [8] C. Alcock, E. Farhi, and A. Olinto, Astrophys. J. **310**, 261 (1986); P. Haensel, J.L. Zdunik, and R. Schaeffer, Astron. Astrophys. **160**, 121 (1986).
- [9] J. Madsen and J.M. Larsen, Phys. Rev. Lett. **90**, 121102 (2003); M. Rybczynski, Z. Włodarczyk, and G. Wilk, Nucl. Phys. Proc. Suppl. **151**, 341 (2006).
- [10] V.V. Usov, Phys. Rev. Lett. **80**, 230 (1998).
- [11] D. Page and V.V. Usov, Phys. Rev. Lett. **89**, 131101 (2002).
- [12] P. Jaikumar, S. Reddy and A.W. Steiner, Phys. Rev. Lett. **96**, 041101 (2006).
- [13] M.G. Alford, K. Rajagopal, S. Reddy, and A.W. Steiner, Phys. Rev. D **73**, 114016 (2006).
- [14] K. Rajagopal and F. Wilczek, Phys. Rev. Lett. **86**, 3492 (2001).
- [15] J. Madsen, Phys. Rev. Lett. **87**, 172003 (2001).
- [16] V.V. Usov, Phys. Rev. D **70**, 067301 (2004).
- [17] A. Chodos, R.L. Jaffe, K. Johnson, C.B. Thorn, and V.F. Weisskopf, Phys. Rev. D **9**, 3471 (1974).
- [18] R.K. Bhaduri, *Models of the Nucleon: From Quarks to Soliton* (Addison-Wesley, Redwood City 1988)
- [19] B.V. Carlson and D. Hirata, Phys. Rev. C **62**, 054310 (2000).
- [20] E. Farhi and R.L. Jaffe, Phys. Rev. D **30**, 2379 (1984).
- [21] W.V. Liu and F. Wilczek, Phys. Rev. Lett. **90**, 047002 (2003).
- [22] H. Abuki, T. Hatsuda, K. Itakura, Phys. Rev. D **65**, 074014 (2002).
- [23] T. Tatsumi, M. Yasuhira, and D.N. Voskresensky, Nucl. Phys. A **718**, 359c (2003).
- [24] F. García-Moliner and F. Flores, *Introduction to the theory of solid surfaces* (Cambridge University Press, Cambridge, 1979).
- [25] A. Schmitt, Q. Wang and D.H. Rischke, Phys. Rev. D **69**, 094017 (2004).
- [26] M.G. Alford, J. Berges, and K. Rajagopal, Nucl. Phys. B **571**, 269 (2000)
- [27] D.F. Litim and C. Manuel, Phys. Rev. D **64**, 094013 (2001).
- [28] E.P. Gilson and R.L. Jaffe, Phys. Rev. Lett. **71**, 332 (1993).
- [29] B.C. Parija, Phys. Rev. C **48**, 2483 (1993).
- [30] J. Madsen, arXiv:astro-ph/0612784 (2006).
- [31] D.A. Varshalovich, A.N. Moskalev, and V.K. Khersonskii, *Quantum Theory of Angular Momentum* (World Scientific, Singapore 1988).
- [32] M.G. Alford, J. Berges, and K. Rajagopal, Nucl. Phys. B **558**, 219 (1999).
- [33] S. Yasui and A. Hosaka, Phys. Rev. D **74**, 054036 (2006).